

Photometric light curve studies: potential bias induced by exposure time

Dezi Liu ¹★, Zuhui Fan ¹†

¹South-Western Institute For Astronomy Research, Yunnan University, Kunming 650500, China

Accepted XXX. Received YYY; in original form ZZZ

ABSTRACT

In photometric observations, the flux averaged over the preset exposure time is usually used as the representation of an object’s true flux at the middle of the exposure interval. For the study of transients and variables, it is also the default manner to build the light curves. In this work, we investigate the effect of this common practice on quantifying the photometric light curves. Our analysis shows that the flux averaged over the exposure time is not necessarily identical to the true flux so that potential bias may be introduced. The overall profile of the true light curve tends to be flattened by the exposure time. In addition, it is found that the peak position and photometric color can also be altered. We then discuss the impacts of the bias induced by exposure time on the light curves of stellar flares, periodic stars, and active galactic nuclei (AGNs). The bias can lead to an underestimate of the total fluxes of stellar flares which has been noticed in the observational data. For periodic stars that follow a sinusoidal light curve, the bias does not affect the period and peak position, but can result in the peak flux being underestimated. Meanwhile, the bias can result in steeper structure function at short timescales for AGN light curves. To obtain unbiased physical parameter estimates from the light curves, our analysis indicates that it is essential to account for this bias, particularly for transients and variables with very short timescales.

Key words: methods: miscellaneous – stars: variables: general – stars: flare

1 INTRODUCTION

Many astronomical objects in the Universe exhibit a variety of dynamic phenomena, often manifesting as variations in brightness or dramatic explosions over different timescales. Based on the types of variability, these objects can be broadly categorized into two groups: transients and variables (LSST Science Collaboration et al. 2009; Hambleton et al. 2023). Transients are objects whose brightness undergoes a sudden change and lasts for only a limited span of time, ranging from milliseconds to years. Examples include supernovae, tidal disruption events, and stellar flares (e.g., Hillebrandt & Niemeyer 2000; Smartt 2009; Lodato & Rossi 2011; Kowalski 2024). In contrast, variables are generally referred to as objects that show persistent brightness variation over various timescales without significantly changing their physical nature, such as pulsating stars and eclipsing binary stars (Eyer & Mowlavi 2008). A large number of observations have indicated that these dynamic phenomena are prevalent in the Universe. The datasets obtained from these observations are constantly updating our understanding of the physical mechanisms concerning the structure, composition and internal activity of these objects (van Velzen et al. 2021; Eyer et al. 2023; Rigault et al. 2024).

The flux variation of these objects under sequential observations is generally referred to as light curve, which is a time series of discrete measurements. To extract the statistical metrics (e.g., amplitudes, colors, etc.) that describe the morphological and temporal proper-

ties of the light curve without bias, accurate measurements are very important. In regard to the observations, however, many factors can affect the measurement accuracy, e.g. the observing strategies, facility status, weather conditions, data processing methods, and so forth. The temporal resolution, as a potential bias source, is tightly related to the observing strategies. Generally, the temporal resolution consists of two aspects: observing cadence (or sampling rate) and exposure time. The observing cadence defines the time interval between two sequential exposures, while the exposure time is the duration that a detector is uninterruptedly exposed to the target object or a patch of sky. The cadence and exposure time are observationally coupled. High cadence observation usually corresponds to short single exposure time, and vice versa. In most observations, the cadence includes not only irregular diurnal, lunar, and seasonal gaps but also additional overheads required for routine activities such as filter changes, detector readout, and telescope slew (Tonry et al. 2018; Ivezić et al. 2019). Consequently, the cadence is typically uneven and longer than the exposure time. Notable exceptions are observations from missions like *Kepler* (Borucki et al. 2010) and *TESS* (Ricker et al. 2015), which exhibit minimal overheads due to their specialized detector designs. In these cases, the exposure time can be considered virtually identical to the cadence¹.

The cadence and exposure time can impose different effects on the observed light curve. The cadence may induce shape deviation from the true light curve due to the discreteness of time sampling. As mentioned above, the cadence is usually unevenly spaced in observation,

★ E-mail: adzliu@ynu.edu.cn (SWIFAR)

† E-mail: zuhuifan@ynu.edu.cn (SWIFAR)

¹ In this paper, we use the term exposure time instead of the commonly used cadence for the *Kepler* and *TESS* light curve.

and can lead to remarkable aliasing in analyzing the periodic light curve (VanderPlas 2018). As for the exposure time, the photometric flux measured within a specified exposure time is an integral value. This makes the variation within the exposure smeared out so that the observed shape of the light curve may also deviate from the true case. The deviation is expected to depend on the profile of the true light curve and the duration of an exposure time. Recently, several studies compared the light curves of stellar flares observed with both long exposure time and short exposure time, and concluded that systematic differences exist on the derived parameters (Yang et al. 2018; Howard & MacGregor 2022). It was found that the flare energy and peak amplitude were underestimated by 25% and 60%, respectively, while the flare duration overestimated by 50% for the long exposure light curves.

With the development of time-domain astronomy, accurate light curve measurements, which are the basis of further study the underlying astrophysics, become crucial. However, few works have discussed the potential bias induced by the temporal resolution in terms of general light curve analysis. Ideally, as discussed above, observations with short exposure and high cadence are desirable to extract the accurate light curve without introducing significant bias. For bright objects, that is sometimes feasible. But for faint objects, it is not always achievable if high signal-to-noise ratio is required. In this case, exposure times of several minutes or longer are usually applied for these objects. Therefore, understanding any potential systematic effects of temporal resolution on quantifying the light curve is important, particularly for upcoming large sky surveys, e.g. the Vera Rubin Observatory Legacy Survey of Space and Time (LSST; Ivezić et al. 2019), which are expected to observe more transients and variables with unprecedented accuracy (Hambleton et al. 2023).

Since the cadence and exposure time are closely related, in this work, we mainly focus on the study of the impacts of exposure time on quantifying the light curve. The paper is structured as follows: in Section 2, we present the bias induced by the exposure time with detailed mathematical analysis. Three examples are then discussed in Section 3. Finally, in Section 4, brief discussions and conclusions are given. In this work, we do not consider noise sources in observational data, such as shoot noise or other stochastic sources resulting from the instruments and measurements.

2 BIAS INDUCED BY EXPOSURE TIME

In photometric observations, the flux of an astronomical object needs to be measured in a specified time interval $[t_1, t_2]$, usually referred to as exposure time, under a given filter. In most light curve analyses, the flux averaged over the exposure time is generally regarded as the flux observed at the middle of the interval $t_m = (t_1 + t_2)/2$. However, this intuitive assumption has never been carefully investigated. In this section, we will explore this assumption with detailed mathematical calculations.

To start with, we assume that the spectral energy distribution $s_\nu(t)$ of a given astronomical object, in unit of $\text{erg s}^{-1} \text{cm}^{-2} \text{Hz}^{-1}$, varies as a function of time t . In the meantime, $s_\nu(t)$ itself is a function of frequency ν . The true flux of the object observed at t_m is the integral of $s_\nu(t_m)$ and the filter transmission curve R_ν , which is

$$f(t_m) = Z_f \int_0^{+\infty} s_\nu(t_m) R_\nu \frac{d\nu}{\nu}, \quad (1)$$

where Z_f is the flux zeropoint determined by the telescope and detector characteristics (Burke et al. 2018). We note that the filter transmission curve R_ν incorporates contributions from multiple causes,

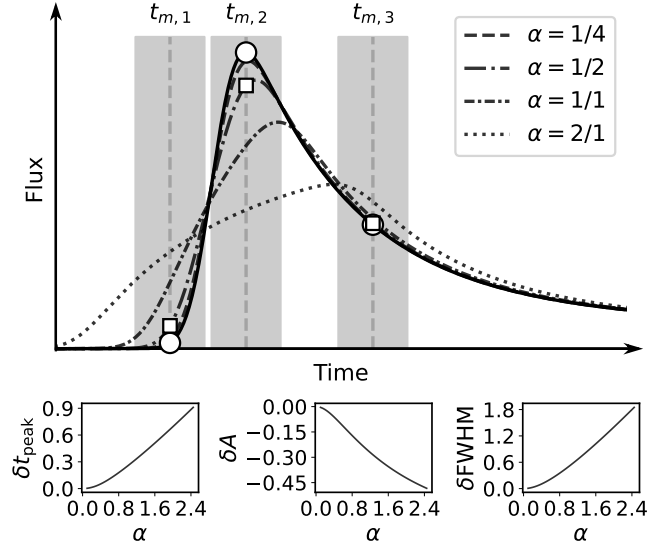


Figure 1. Top panel: a sketch map to show the Δt -bias. The solid line is an empirical light curve template of white-light stellar flares. Other lines represent the time-averaged light curves. Three vertical dashed lines illustrate an example pattern of cadence at times $t_{m,1}$, $t_{m,2}$, and $t_{m,3}$. The width of each shaded region is equal to the exposure time $\Delta t = \text{FWHM}/2$. The circles represent the resulting discrete light curve for our flare template, while the squares represent the discrete light curve with $\alpha = 1/2$ after incorporating Δt -bias. Bottom panel: the differences of the profile parameters (t_{peak} , A , and FWHM) relative to those of the template as a function of exposure time.

including the Earth's atmosphere, telescope optics, filter glass, and detector (for a detailed definition, see, e.g., Hogg 2022). The magnitude is then defined as

$$m(t_m) = -2.5 \log_{10} \left[\frac{\int_0^{+\infty} s_\nu(t_m) R_\nu \frac{d\nu}{\nu}}{\int_0^{+\infty} g_\nu^{\text{ref}} R_\nu \frac{d\nu}{\nu}} \right],$$

where g_ν^{ref} is the time-independent spectral energy distribution of a standard reference source, which is the spectrum of Vega for Vega magnitude, or a hypothetical constant source with $g_\nu^{\text{ref}} = 3631 \text{ Jy}$ at all frequencies for AB magnitude (Oke & Gunn 1983). Similarly, the time-averaged flux in the time interval $[t_1, t_2]$ can be calculated through

$$\begin{aligned} f_s(t_m) &= Z_f \frac{1}{\Delta t} \int_{t_m - \Delta t/2}^{t_m + \Delta t/2} dt \int_0^{+\infty} s_\nu(t) R_\nu \frac{d\nu}{\nu} \\ &= \frac{1}{\Delta t} \int_{t_m - \Delta t/2}^{t_m + \Delta t/2} f(t) dt, \end{aligned} \quad (2)$$

where the time duration Δt , defined as $\Delta t = t_2 - t_1$, is the exposure time.

In observation, we can never measure the true flux $f(t_m)$ because any facility needs a given time duration to complete an exposure, i.e. $\Delta t > 0$. Instead, the time-averaged flux $f_s(t_m)$ is the direct observable. When assembling the light curve of an astronomical object and performing quantitative analysis, we intuitively use $f_s(t_m)$ as a representation of the potentially real $f(t_m)$. Apparently, when the object is stable and its flux does not vary with time, the true flux and time-averaged flux are equal, i.e. $f(t_m) = f_s(t_m)$. Generally, however, for variables or transients $f_s(t_m)$ and $f(t_m)$ are not necessarily identical. As a result, this assumption may lead to systematic bias

in interpreting the light curves. In the following analysis, we denote this potential bias as exposure time bias (Δt -bias).

Firstly, under the limit of Δt approaching to zero the fundamental calculus theorem tells us that

$$f(t_m) = \lim_{\Delta t \rightarrow 0} f_s(t_m). \quad (3)$$

Or equivalently, if we define ω_t as the typical timescale of $f(t_m)$, e.g. the full width at half-maximum (FWHM), and a scale parameter $\alpha \equiv \Delta t/\omega_t$, equation (3) is also satisfied under the limit of α approaching to zero. Therefore, it is expected that $f_s(t_m)$ and $f(t_m)$ will be very close if the exposure time (Δt) or the relative exposure time (α), when compared to the timescale of the light curve, is short.

To quantify the Δt -bias in more general case, the simple way is to compare the difference between the two fluxes, which can be defined as

$$\Delta f(t_m) = f_s(t_m) - f(t_m) = \frac{1}{\Delta t} \int_{t_m - \Delta t/2}^{t_m + \Delta t/2} [f(t) - f(t_m)] dt. \quad (4)$$

For a given light curve, the flux variations typically display sequential brightening and darkening phases, such as the periodic stars and various transients. Mathematically, these different phases can be modeled by the sum of convex and concave functions (e.g. Yuille & Rangarajan 2003). Then we can apply the classical Hermite-Hadamard (HH) inequality (e.g. Niculescu & Persson 2003) to derive the relationship between $f(t_m)$ and $f_s(t_m)$. When the light curve is convex in a given time interval, the HH inequality states that $f(t_m) < f_s(t_m)$. And we have $f(t_m) > f_s(t_m)$ in the case of a concave light curve. In addition, if and only if the light curve is a linear function of time, the equality holds. In summary, we have

- $\Delta f(t_m) > 0$ if $f(t_m)$ is convex,
- $\Delta f(t_m) < 0$ if $f(t_m)$ is concave, and
- $\Delta f(t_m) = 0$ if $f(t_m)$ is linear.

The detailed mathematical proof is provided in Appendix A. It is observationally evident that the light curves of most real astronomical objects show non-linear dependence on time. Therefore, the time-averaged flux $f_s(t_m)$ will be a biased measure of the true flux $f(t_m)$. From the discussion above, it is expected that the Δt -bias tends to flatten the true light curve. And the difference $\Delta f(t_m)$ depends on the specific shape of the light curve and the exposure time as indicated by equation (4).

Furthermore, we find that the Δt -bias can also alter the peak position. Assuming the peak positions are t_{peak} and $t_{s, \text{peak}}$ for the true light curve and time-averaged light curve, respectively, the mathematical proof (see Appendix B) indicates that their difference δt_{peak} (defined as $t_{s, \text{peak}} - t_{\text{peak}}$) always satisfies $|\delta t_{\text{peak}}| < \Delta t/2$. For light curves with fast rise and then slow decay phases around the peak, $t_{s, \text{peak}}$ will shift rightwards ($t_{s, \text{peak}} > t_{\text{peak}}$). While for light curves with slow rise and then fast decay phases around the peak, $t_{s, \text{peak}}$ shifts leftwards ($t_{s, \text{peak}} < t_{\text{peak}}$). And if the light curve is axisymmetric with respect to $t_m = t_{\text{peak}}$, the peak position does not change so that we have $t_{s, \text{peak}} = t_{\text{peak}}$.

An illustration of the Δt -bias is shown in the top panel of Fig. 1. The solid line represents an empirical light curve template of white-light stellar flares constructed by using the 1-minute exposure data from *Kepler* mission (Tovar Mendoza et al. 2022). It is simple to prove that in the early rise and late decay phases, the light curve is convex, while it is concave around the peak. In this model, three free parameters are used to describe the general profile of a flare light curve: the peak time t_{peak} , flux amplitude A , and FWHM. For the default template as shown in the figure, we have $t_{\text{peak}} = -0.0026$, $A = 0.9502$, and $\text{FWHM} = 1.0867$, respectively. Here we define the

scale parameter as $\alpha = \Delta t/\text{FWHM}$. The time-averaged light curves derived by equation (2) with different exposure times are shown in the top panel of Fig. 1. It can be seen that significant deviations present in the fast rise and peak phases between the true and time-averaged fluxes. In the late decay phase, the deviations become smaller because the light curves tend to be linear over time. The Δt -bias does make the profile of the light curve flatter as the increase of exposure time. In addition, as we have demonstrated, as the increase of exposure time, not only does the amplitude of the peak get smaller, but the position of the peak systematically shifts rightwards. In the bottom panel of Fig. 1, we show the differences of the parameters t_{peak} , A , and FWHM relative to those of the template light curve as a function of exposure time.

We note that the light curves of many other transient events, such as supernovae and fast blue optical transients (Perley et al. 2020; Ho et al. 2023), also present the similar profile as the stellar flares, i.e. a fast rise phase and then a following slow decay phase. Therefore, the results described here are also expected to hold for them.

In addition to the bias induced by exposure time, observing cadence can also affect the analysis of photometric light curves. The cadence does not alter the true flux, but imposes a finite rate of sampling, making the observed light curves discrete. Mathematically, this discreteness can be described by a pointwise product of the true light curve $f(t)$ and a Dirac Comb window function $W_{\{t_{m,i}\}}(t)$, which is a sequence of Dirac delta functions spaced with a given time series $\{t_{m,i}\}$ where i ranges from 1 to n , and n is the total number of exposures (VanderPlas 2018; Ivezić et al. 2020). Specifically, the discrete light curve can be written as

$$\mathcal{F}(t) = f(t) W_{\{t_{m,i}\}}(t) = \sum_{i=1}^n f(t_{m,i}) \delta(t - t_{m,i}), \quad (5)$$

where $\delta(t)$ is the Dirac delta function at time t . As we mentioned earlier, the cadence is usually nonuniform because of the influences of observing time windows and instrumental operations. In the context of spectral analysis, the cadence may result in aliasing effects that hinder the accurate quantification of the underlying true signals. For more discussions on this aspect, we direct interested readers to VanderPlas (2018) and references therein. In Fig. 1, the vertical dashed lines illustrate a window function $W(t)$, and the circles depict the resulting discrete light curve for our flare template. In this example, the window function can be expressed as $W_{\{t_{m,i}\}}(t) = \sum_{i=1}^3 \delta(t - t_{m,i})$.

However, we emphasize that in the presence of Δt -bias, the cadence-induced pointwise product in equation (5) should be modified. That is, the real observed light curve must contain effects due to both exposure time and cadence. Thus, we can substitute the true flux with the time-averaged flux that is obtained from equation (2), and express the observed discrete light curve as

$$\mathcal{F}_s(t) = \sum_{i=1}^n f_s(t_{m,i}) \delta(t - t_{m,i}). \quad (6)$$

As illustrated in Fig. 1, under the given window function $W_{\{t_{m,i}\}}(t)$ and exposure time Δt , the discrete light curve with $\alpha = 1/2$ (i.e., $\Delta t = \text{FWHM}/2$ as defined before) is supposed to be observed as squares instead of circles.

Besides the impact on light curve morphology, Δt -bias can also distort color measurements. Astronomical color is defined as the magnitude difference between two filters. For filters X and Y , the color $c_{XY}(t_m)$ at time t_m is calculated as $c_{XY}(t_m) = m^X(t_m) - m^Y(t_m)$, where $m^X(t_m)$ and $m^Y(t_m)$ are magnitudes for the two filters. Conventionally, the wavelength of filter X is shorter than that of Y . Because the true light curve of a transient or variable is usually

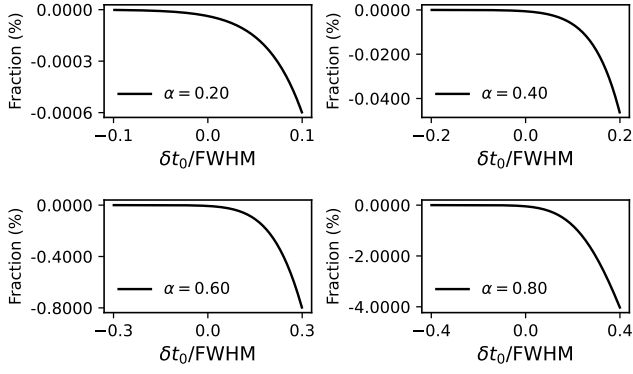


Figure 2. Fraction of the total flux as a function of relative time offset. The four panels show the results with different exposure times.

color-dependent, and the exposure times for different filters vary in real observations, we can, without loss of generality, substitute equation (2) into this color equation to yield

$$\begin{aligned}
 c_{XY}(t_m) &= -2.5 \log_{10}(f_s^X(t_m)) + 2.5 \log_{10}(f_s^Y(t_m)) \\
 &= -2.5 \log_{10} \left[\frac{\int_{t_m - \Delta t^X/2}^{t_m + \Delta t^X/2} f^X(t) dt}{\int_{t_m - \Delta t^Y/2}^{t_m + \Delta t^Y/2} f^Y(t) dt} \right] + 2.5 \log_{10} \left(\frac{\Delta t^X}{\Delta t^Y} \right),
 \end{aligned} \tag{7}$$

where $f^X(t)$ and $f^Y(t)$ denote the true light curves for filters X and Y , respectively. The corresponding time-averaged fluxes are $f_s^X(t_m)$ and $f_s^Y(t_m)$, with exposure times of Δt^X and Δt^Y . This equation reveals that the color also depends on the exposure time Δt . Even if $\Delta t^X = \Delta t^Y$, the first term remains a function of Δt . Furthermore, we note that observations in different filters generally have distinct cadences or window functions. To calculate the colors of a transient or variable and deduce the associated physical properties, we must interpolate or model the light curves of different filters to a common time grid. Therefore, properly incorporating the Δt -bias will become necessary.

In summary, we stress that the Δt -bias induced by exposure time is non-negligible for light curve analysis, particularly when the exposure time is comparable to the timescale of a target transient or variable. Additionally, cadence can introduce extra computational complexity. To extract unbiased physical parameters, one feasible approach is to incorporate the Δt -bias and cadence directly into the theoretical light curves or colors, and then fit them to observational data.

3 CASE STUDIES

In this section, we further study the Δt -bias for the light curves of stellar flares, periodic stars, and AGNs. In what follows, we assume that the exposure time Δt is always constant and there are no additional overheads or other gaps between two sequential exposures.

3.1 Stellar Flares

We start with the discussion of the empirical stellar flare template as shown in Fig. 1. The initial eruption time of the stellar flare is at $t_0 = -1$, and the total flux f_{tot} estimated by the integral under the light curve is 2.0409. Besides the aforementioned effects induced by

the Δt -bias, we further investigate the total integrated flux $f_{s, \text{tot}}$ of the time-averaged light curve. Since the light curve is discrete, the trapezoidal rule is adopted to estimate the total flux, which is

$$f_{s, \text{tot}} = \sum_{i=1}^{n-1} \frac{f_s(t_{m, i}) + f_s(t_{m, i+1})}{2} \Delta t, \tag{8}$$

where i is the i -th exposure and n is the total number of exposures. Because exposures before t_0 do not contribute to the total flux estimate, we can unambiguously set t_0 to be within the first exposure interval $[t_{m, 1} - \Delta t/2, t_{m, 1} + \Delta t/2]$, and define the relative offset as $\delta t_0 = t_{m, 1} - t_0$. Similarly, we denote the eruption end time as t_e , and set it to be within the last exposure interval $[t_{m, n} - \Delta t/2, t_{m, n} + \Delta t/2]$. The relative time offset between t_e and $t_{m, n}$ is $\delta t_e = t_{m, n} - t_e$. Immediately, we have the inequalities $|\delta t_0| < \Delta t/2$ and $|\delta t_e| < \Delta t/2$. Based on these definitions, we can derive the relationship between $f_{s, \text{tot}}$ and f_{tot} (see Appendix C), which follows

$$\begin{aligned}
 f_{s, \text{tot}} &= f_{\text{tot}} - \frac{1}{2} [f_s(t_{m, 1}) + f_s(t_{m, n})] \Delta t \\
 &= f_{\text{tot}} - \frac{1}{2} \left[\int_{t_{m, 1} - \delta t_0}^{t_{m, 1} + \Delta t/2} f(t) dt + \int_{t_{m, n} - \Delta t/2}^{t_{m, n} - \delta t_e} f(t) dt \right].
 \end{aligned} \tag{9}$$

Equation (9) demonstrates that $f_{s, \text{tot}}$ underestimates the true total flux f_{tot} . The degree of underestimation depends on the time offsets δt_0 and δt_e , the exposure time Δt , and the inherent profile of the light curve. Only under the extreme case that the initial eruption time of a stellar flare t_0 is completely coincident with the end time of the first exposure (i.e., $t_0 = t_{m, 1} + \Delta t/2$) and the end time t_e coincides with the start of the last exposure (i.e., $t_e = t_{m, n} - \Delta t/2$), $f_{s, \text{tot}}$ can be an unbiased estimator of f_{tot} . However, equation (9) also reveals that a simple correction factor $[f_s(t_{m, 1}) + f_s(t_{m, n})] \Delta t/2$ can be added to $f_{s, \text{tot}}$ to calculate the corrected total flux. Fig. 2 illustrates the fraction of underestimation for different exposure times for the stellar flare template. In each of the four panels, the horizontal axis is the relative time offset δt_0 which is normalized to the FWHM, and the vertical axis is the flux fraction, defined as $f_{s, \text{tot}}/f_{\text{tot}} - 1$. As a practical example, Yang et al. (2018) reported that the flare energies estimated from *Kepler* long-exposure data are systematically underestimated by 25% when compared to those obtained from short-exposure data. This can be partially explained by Fig. 2, which illustrates that the fraction of underestimation indeed increases with the increase of exposure time. In addition, equation (9) also indicates that accurately determining the eruption start time t_0 and end time t_e (or the flare duration $t_e - t_0$) is crucial for unbiased total flux calculation. However, Yang et al. (2018) found systematic differences in these parameters. For more discussions on the underestimation, interested readers are referred to their work.

To further investigate the Δt -bias for practical light curve analysis, we compare the light curve fitting results with and without taking the exposure time into account. We firstly simulate stellar flare light curves with different exposure times. The parameters of the fiducial true light curve profile are set to be $A = 9.469$ and $\text{FWHM} = 6.540$ minutes. These values represent the best-fit means (Xing et al. 2024) for the flare samples from Howard & MacGregor (2022). In addition, we arbitrarily set the peak time as $t_{\text{peak}} = 0.0$ minute. The red line in each panel of Fig. 3 displays the fiducial true light curve profile. We then generate the time-averaged light curves using equation (2) with exposure times $\Delta t = 120$ s, 300 s, and 600 s, respectively. The noise of each light curve is assumed to follow the Gaussian distribution $N \sim (0, \sigma^2)$, where $\sigma = A/50$, meaning that the signal-to-noise ratio of the peak amplitude is fixed

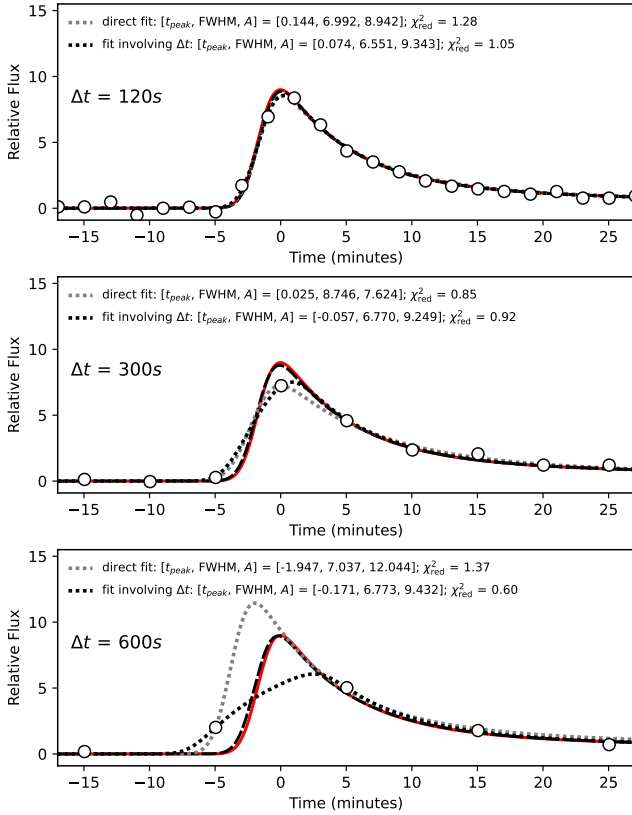


Figure 3. Illustration of the impact of Δt -bias on stellar flare light curve fitting. In each panel, the solid red line is the input fiducial true light curve profile, and the circles represent the simulated light curve with exposure time Δt . The gray dotted line is the result by fitting the simulated data using the parameterized stellar flare profile directly. The black dashed line is the best-fit profile taking the Δt -bias into account, and the black dotted line corresponds to the time-averaged profile (see text for details).

to 50. The final time-averaged light curves with different exposure times are shown as circles in Fig. 3.

Next, we fit these simulated light curves. The gray dotted line in each panel of Fig. 3 represents the result by fitting the data using the parameterized stellar flare profile directly. This is also the generally adopted method in current studies (e.g. Tovar Mendoza et al. 2022; Voloshina et al. 2024). The best-fit parameters are provided in each panel and Table D1. Obviously, the best-fit parameters are not consistent with the fiducial values. On the other hand, in order to take the Δt -bias into account, we substitute the parameterized stellar flare profile into equation (2), i.e., $f(t)$ inside the integral, and derive the best-fit parameters again using the circled data points. The result is shown by the black dashed line in each panel of Fig. 3. The black dotted line corresponds to the profile obtained by the time-averaging of the solid black line. It can be seen that the black dashed line matches the fiducial model much better compared to the gray dotted lines from the direct fitting, though the two methods can both fit the data well and give similar reduced χ^2_{red} . In addition, we note that the direct fitting method tends to give larger deviation from the fiducial model as the exposure time increases. The simulation results indicate that it is indispensable to consider the Δt -bias in the light curve fitting procedures in order to obtain unbiased estimate of the physical quantities.

We then apply the same fitting methods to a real stellar flare occur-

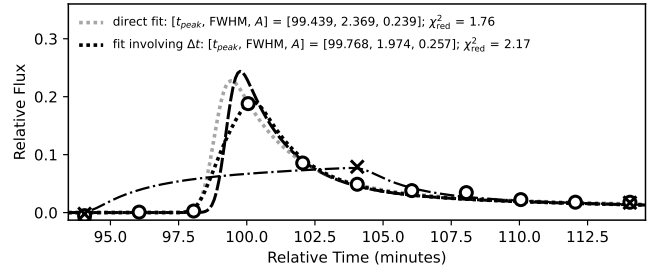


Figure 4. Light curve fitting of a real stellar flare occurring on an M3.5 star (TIC 197829751) observed by *TESS*. The circles and crosses represent the light curves with exposure times of $\Delta t = 120\text{s}$, and 600s , respectively. Same as Fig. 3, the gray dotted line is the best-fit light curve by directly fitting the 120s-exposure data. The black dashed and dotted lines are the best-fit profile when taking the Δt -bias into account, and the corresponding time-averaged profile, respectively. The dash-dotted line represents the predicted 600s-exposure light curve.

ring on an M3.5 star (TIC 197829751) from *TESS* data (Schneider et al. 2019). *TESS* observed the stellar flare with three different exposure times: $\Delta t = 20\text{s}$, 120s , and 600s . Since the stellar flare template is constructed using the 1-minute exposure data from *Kepler* mission, in principle it is not feasible to fit the light curve observed with shorter exposure due to the Δt -bias. This is evident from the poor fit to the peak fluxes as shown in Tovar Mendoza et al. (2022, Fig. 10). Thus we opt to fit only the 120s-exposure light curve, and show the best-fit results in Fig. 4. We note that the parameters estimated by the direct fitting method are identical to that provided by Tovar Mendoza et al. (2022). Similar to the simulation, when involving the Δt -bias, the estimated parameters are different, particularly for the FWHM which decreases from 2.369 minutes to 1.974 minutes. We then integrate the best-fit light curve profile (black dashed line) with the longest exposure time $\Delta t = 600\text{s}$ using equation (2) to predict the corresponding light curve. It can be seen that the prediction (dash-dotted line) is completely consistent with the observed light curve with exposure time of $\Delta t = 600\text{s}$.

3.2 Periodic Stars

For periodic stars, we assume that the true light curve varies periodically by following

$$f(t_m) = A [\sin(2\pi\omega t_m + \phi) + B], \quad (10)$$

where A and B are constants, and required to satisfy $A > 0$ and $B > 1$ to ensure $f(t_m)$ is always positive. In addition, ω is the frequency which is related to the period T by $T = 1/\omega$, and ϕ is the phase. Based on the periodicity of the sine function, the light curve is concave in the interval $t_m \in [k/\omega - \phi/2\pi\omega, k/\omega - (\phi - \pi)/2\pi\omega]$ where k is an integer starting from 0. And it is convex in the interval $[k/\omega - (\phi - \pi)/2\pi\omega, k/\omega - (\phi - 2\pi)/2\pi\omega]$. Inserting the above equation into equation (2), we get

$$f_s(t_m) = A \left[\frac{\sin(\pi\omega\Delta t)}{\pi\omega\Delta t} \sin(2\pi\omega t_m + \phi) + B \right]. \quad (11)$$

By comparing equations (10) and (11), it is found that the period and position of the peak are not affected by the Δt -bias. In addition, the average flux can be calculated by integrating the light curve over a period T . By definition, the average flux of the true light curve $f(t_m)$ is $\int_0^T f(t_m) dt_m / T = AB/T$, and the same value holds for the time-averaged light curve $f_s(t_m)$. That is, the average flux (or

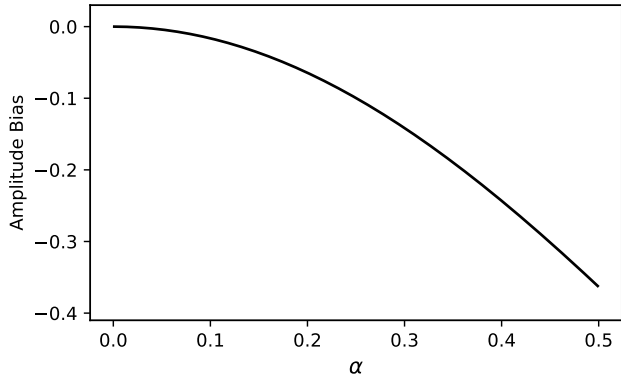


Figure 5. Amplitude bias as a function of relative exposure time for periodic stars with sinusoidal light curve.

equivalently, the average magnitude) is also unchanged. But an extra term $\sin(\pi\omega\Delta t)/(\pi\omega\Delta t)$ appears in the time-averaged flux $f_s(t_m)$, meaning that the amplitude gets smaller since $\sin(\pi\omega\Delta t)/(\pi\omega\Delta t) < 1$ always holds when $\Delta t > 0$. By defining the relative time scale $\alpha = \Delta t/T = \omega\Delta t$, the dependence of the amplitude bias on the parameter α , which is $\sin(\pi\alpha)/(\pi\alpha) - 1$, is presented in Fig. 5. As seen in the figure, it is expected that the Δt -bias will be significant for the study of short period stars with periods of several minutes or shorter (Baran et al. 2023, 2024).

One of the important applications of periodic stars is to determine cosmic distances, such as through the period-color-luminosity relation based on the Cepheid or RR Lyrae variables (e.g. Bhardwaj 2020). Generally, the color and luminosity of such a variable are derived from the average magnitudes of the light curves obtained using different filters, through Fourier decomposition or template fitting (Schaltenbrand & Tammann 1971; Sesar et al. 2010). As we have proved, both the period and the average magnitude remain unaffected by the Δt -bias. In principle, it is expected that the period-color-luminosity relation is also unaffected. However, it becomes necessary to account for the Δt -bias when we investigate any relation related to amplitude, such as the period-amplitude relation (e.g. Bhardwaj 2020).

In addition, it is worth further discussing the template fitting method. It has been widely applied in deriving the average magnitude and amplitude of a light curve (Sesar et al. 2010; Savino et al. 2022). In particular, when the light curve is sparsely sampled, the template fitting method is more reliable (Kovács & Kupi 2007). However, these template light curves are constructed from observations with specified exposure times and cadences, which already incorporate the Δt -bias. When fitting these templates to light curves, which are usually collected from different observations with distinct exposure times and cadences, potential biases may be introduced into the derived parameters. Detailed investigations are not within the scope of this paper, and we leave them for future studies.

3.3 AGNs

The light curves of AGNs can be described by the damped random walk model (Kelly et al. 2009). For short timescales, the power spectral density (PSD) of the AGN light curves follows $\text{PSD}(f) \propto f^{-\alpha}$, where f is the frequency, and α is the power-law index. In the case of a random walk process, we have $\alpha = 2$. Another way to model the variability of AGNs is the structure function (SF) which

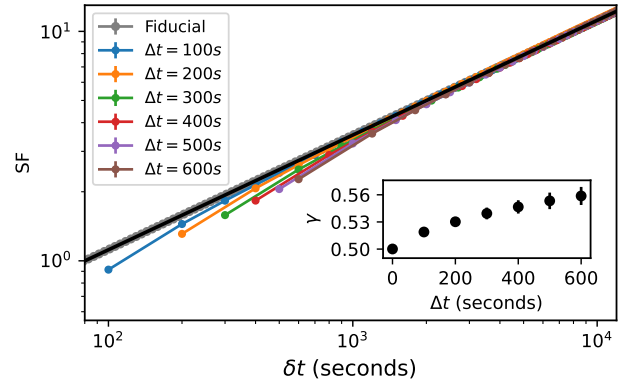


Figure 6. Comparison of the SFs with different exposure times. For a given exposure time, the SF is an average of 100 individual SFs. The gray dots with error bars and black line represent the fiducial and expected true SF with $\gamma = 0.5$, respectively. The power-law index γ as a function of exposure time is shown in the inset.

is defined as the flux (or magnitude) difference as a function of time lag δt (e.g. Kozłowski 2016):

$$\text{SF}(\delta t) = \sqrt{\frac{1}{N_{\delta t, \text{pair}}} \sum_{i=1}^{N_{\delta t, \text{pair}}} (f(t) - f(t + \delta t))^2}, \quad (12)$$

where $N_{\delta t, \text{pair}}$ is the number of pairs for a given δt , and f is the flux. For short timescale, the SF also follows a power-law form $\text{SF}(\delta t) \propto \delta t^\gamma$, and $\gamma = 0.5$ for the damped random walk model. Here we investigate how the Δt -bias affects the determination of the power-law index γ of the SF.

We use *Stingray*, a toolkit developed by Huppenkothen et al. (2019), to generate the simulated AGN light curves by following the random walk process. The mean and standard deviation of the fiducial light curves are set to be 100.0 and 0.5, respectively. In addition, since the time resolution cannot be infinitesimal, we set it to be 0.1 seconds. In total, 100 fiducial light curves are generated with different random seeds. We then get the light curves with different exposure times by following equation (2) and further calculate the corresponding SFs. For a given exposure time Δt , we average the 100 individual SFs and show the result in Fig. 6. It can be seen that the SFs with different exposure times are all steeper compared to the fiducial SF (gray dots with error bars) and the expected true SF with $\gamma = 0.5$ (black line) at short timescale. The steepness becomes larger as the increase of exposure time. We can also find that the SFs are consistent with the fiducial one at long timescale, indicating that the Δt -bias mostly affects the short-timescale variability of AGNs. To quantify the impact of Δt -bias on the SFs, we fit the averaged SFs with the power-law formula. The upper limit of the fitting is fixed to 0.1 days. The best-fit power-law index γ as a function of exposure time is shown in the inset of Fig. 6. Remarkably, the γ value increases about 12% when the exposure time is 600 s. The results indicate that the explanation about the variability features of AGNs at short timescale should be careful in the presence of Δt -bias, particularly for the study of intra-night variability of AGNs (Wagner & Witzel 1995, and references therein).

4 DISCUSSIONS AND CONCLUSIONS

In this paper, we have analyzed the impacts of the bias induced by exposure time on observed photometric light curves. Mathematical calculations showed that the time-averaged flux with a given exposure time is not necessarily identical to the expected value of the true light curve. The bias or their difference depends on the duration of the exposure time and the specific shape of the true light curve. Generally, when the true light curve is convex in a certain exposure, the time-averaged flux will be larger than the expected true flux. It is smaller when the true light curve is concave. As a result, the exposure time tends to flatten the true light curve and enlarge the characteristic timescale (e.g. the FWHM). Meanwhile, the peak position and photometric color are also altered.

We have discussed the bias for three types of light curves in detail: stellar flares, periodic stars, and AGNs. For the stellar flares, like many other transients, their light curves present three remarkable phases, a fast rise phase, a sharp peak phase, and then a slow decay phase. Besides the systematic underestimation of the peak flux and shift of the peak position, the exposure time bias can also cause the total integrated flare flux to be underestimated. The fraction depends on the duration of the exposure time. We further demonstrated the impact of the bias on the morphological parameters that were estimated by fitting both simulated and real observed light curves. For periodic stars, our analysis indicates that the bias will not affect the period and peak position determination, but can give rise to an underestimate of the peak flux. For the AGNs, we calculated the SFs of a set of simulated light curves that follow the random walk process and demonstrated that the exposure time can make the slopes of the SFs steeper at short timescale. It turns out that the steepness is proportional to the exposure time. In addition to the analysis presented here, however, it will be interesting to further explore the impacts of the exposure time bias on other aspects regrading light curve studies, and extend the analysis to many other transients and variables. Moreover, it usually takes even longer exposure times to perform spectroscopic observations for these transients and variables. Thus it is expected that quantifying the bias for the derived parameters from the spectra is also necessary.

We emphasize that the bias is sensitive to the exposure time or the relative exposure time, i.e. the ratio of the exposure time to the typical timescale of the light curve. For variables or transients with long timescale variation, such as stars with period longer than days or supernovae with typical timescale of weeks, the relative exposure time is very small (typically $\Delta t/\omega_t \lesssim 10^{-3}$), and thus the bias is expected to be negligible. However, with the increase of the discoveries of the short period stars and fast transients (Denissenya & Linder 2021; Hambleton et al. 2023; Baran et al. 2023, 2024), it is essential to account for the bias if unbiased physical parameters are desired.

ACKNOWLEDGEMENTS

We thank the anonymous referee for the constructive comments that significantly enhanced the quality of our manuscript. Dezi Liu acknowledges the supports from NSFC under the grant of 12103043, and National Key R&D Program of China No. 2022YFF0503404. Zuhui Fan is supported by NSFC under 11933002, U1931210 and 11333001.

This paper includes data collected with the TESS mission, obtained from the MAST data archive at the Space Telescope Science Institute (STScI). Funding for the TESS mission is provided by the NASA

Explorer Program. STScI is operated by the Association of Universities for Research in Astronomy, Inc., under NASA contract NAS 5–26555. This research made use of Lightkurve, a Python package for Kepler and TESS data analysis (Lightkurve Collaboration et al. 2018). This work made use of Astropy:² a community-developed core Python package and an ecosystem of tools and resources for astronomy (Astropy Collaboration et al. 2013, 2018, 2022). Besides, this work has also used the following Python packages: numpy (Harris et al. 2020), scipy (Virtanen et al. 2020), matplotlib (Hunter 2007), and Stingary (Huppenkothen et al. 2019).

DATA AVAILABILITY

The data underlying this article will be shared on reasonable request to the corresponding authors.

REFERENCES

- Astropy Collaboration et al., 2013, *A&A*, **558**, A33
 Astropy Collaboration et al., 2018, *AJ*, **156**, 123
 Astropy Collaboration et al., 2022, *ApJ*, **935**, 167
 Baran A. S., et al., 2023, *A&A*, **669**, A48
 Baran A. S., Charpinet S., Østensen R. H., Reed M. D., Van Grootel V., Lyu C., Teltng J. H., Németh P., 2024, *arXiv e-prints*, p. arXiv:2403.02384
 Bhardwaj A., 2020, *Journal of Astrophysics and Astronomy*, **41**, 23
 Borucki W. J., et al., 2010, *Science*, **327**, 977
 Burke D. L., et al., 2018, *AJ*, **155**, 41
 Denissenya M., Linder E. V., 2021, *The Open Journal of Astrophysics*, **4**, 14
 Eyer L., Mowlavi N., 2008, in *Journal of Physics Conference Series*. IOP, p. 012010 (arXiv:0712.3797), doi:10.1088/1742-6596/118/1/012010
 Eyer L., et al., 2023, *A&A*, **674**, A13
 Hambleton K. M., et al., 2023, *PASP*, **135**, 105002
 Harris C. R., et al., 2020, *Nature*, **585**, 357
 Hillebrandt W., Niemeyer J. C., 2000, *ARA&A*, **38**, 191
 Ho A. Y. Q., et al., 2023, *ApJ*, **949**, 120
 Hogg D. W., 2022, *arXiv e-prints*, p. arXiv:2206.00989
 Howard W. S., MacGregor M. A., 2022, *ApJ*, **926**, 204
 Hunter J. D., 2007, *Computing in Science & Engineering*, **9**, 90
 Huppenkothen D., et al., 2019, *ApJ*, **881**, 39
 Ivezić Ž., et al., 2019, *ApJ*, **873**, 111
 Ivezić Ž., Connolly A. J., VanderPlas J. T., Gray A., 2020, *Statistics, Data Mining, and Machine Learning in Astronomy. A Practical Python Guide for the Analysis of Survey Data*, Updated Edition. Princeton University Press, doi:10.1515/9780691197050
 Kelly B. C., Bechtold J., Siemiginowska A., 2009, *ApJ*, **698**, 895
 Kovács G., Kupi G., 2007, *A&A*, **462**, 1007
 Kowalski A. F., 2024, *Living Reviews in Solar Physics*, **21**, 1
 Kozłowski S., 2016, *ApJ*, **826**, 118
 LSST Science Collaboration et al., 2009, *arXiv e-prints*, p. arXiv:0912.0201
 Lightkurve Collaboration et al., 2018, *Lightkurve: Kepler and TESS time series analysis in Python*, *Astrophysics Source Code Library* (ascl:1812.013)
 Lodato G., Rossi E. M., 2011, *MNRAS*, **410**, 359
 Niculescu C. P., Persson L.-E., 2003, *Real Analysis Exchange*, **29**, 663
 Oke J. B., Gunn J. E., 1983, *ApJ*, **266**, 713
 Perley D. A., et al., 2020, *ApJ*, **904**, 35
 Ricker G. R., et al., 2015, *Journal of Astronomical Telescopes, Instruments, and Systems*, **1**, 014003
 Rigault M., et al., 2024, *arXiv e-prints*, p. arXiv:2409.04346
 Savino A., et al., 2022, *ApJ*, **938**, 101
 Schaltenbrand R., Tammann G. A., 1971, *A&AS*, **4**, 265

² <http://www.astropy.org>

- Schneider A. C., Shkolnik E. L., Allers K. N., Kraus A. L., Liu M. C., Weinberger A. J., Flagg L., 2019, *AJ*, **157**, 234
- Sesar B., et al., 2010, *ApJ*, **708**, 717
- Smartt S. J., 2009, *ARA&A*, **47**, 63
- Tonry J. L., et al., 2018, *PASP*, **130**, 064505
- Tovar Mendoza G., Davenport J. R. A., Agol E., Jackman J. A. G., Hawley S. L., 2022, *AJ*, **164**, 17
- VanderPlas J. T., 2018, *ApJS*, **236**, 16
- Virtanen P., et al., 2020, *Nature Methods*, **17**, 261
- Voloshina A. S., et al., 2024, *arXiv e-prints*, p. arXiv:2404.07812
- Wagner S. J., Witzel A., 1995, *ARA&A*, **33**, 163
- Xing K., et al., 2024, *ApJS*, **271**, 57
- Yang H., Liu J., Qiao E., Zhang H., Gao Q., Cui K., Han H., 2018, *ApJ*, **859**, 87
- Yuille A. L., Rangarajan A., 2003, *Neural Computation*, **15**, 915
- van Velzen S., et al., 2021, *ApJ*, **908**, 4

APPENDIX A: HERMITE-HADAMARD INEQUALITY

The Hermite-Hadamard inequality states that for a given convex function $g(x)$, in the interval $[a, b] \rightarrow \mathbb{R}$, we have

$$g\left(\frac{a+b}{2}\right) \leq \frac{1}{b-a} \int_a^b g(x) dx. \quad (\text{A1})$$

More complete form and relevant proof can be found in Niculescu & Persson (2003) and references therein. Similarly, if $g(x)$ is a concave function, then

$$g\left(\frac{a+b}{2}\right) \geq \frac{1}{b-a} \int_a^b g(x) dx. \quad (\text{A2})$$

In both cases, equality holds only for functions of the form $g(x) = kx + d$, where k and d are real numbers.

Substituting equation (1) and equation (2) into the Hermite-Hadamard inequality, it is straightforward to prove that when the light curve is convex, we have

$$\begin{aligned} f(t_m) &= f\left(\frac{t_m - \Delta t/2 + t_m + \Delta t/2}{2}\right) \\ &\leq \frac{1}{\Delta t} \int_{t_m - \Delta t/2}^{t_m + \Delta t/2} f(t) dt \\ &= Z_f \frac{1}{\Delta t} \int_{t_m - \Delta t/2}^{t_m + \Delta t/2} dt \int_0^\infty s_\nu(t) R_\nu \frac{d\nu}{\nu} \\ &= f_s(t_m), \end{aligned} \quad (\text{A3})$$

i.e., $f(t_m) \leq f_s(t_m)$. When the light curve is concave, it can be demonstrated that $f(t_m) \geq f_s(t_m)$. Again, the equality holds only in the case of $f(t_m) = kt_m + d$, namely, when the light curve is a linear function of time.

APPENDIX B: PEAK POSITION SHIFT

For a light curve with a single peak, we assume that the peak positions of $f(t_m)$ and $f_s(t_m)$ are t_{peak} and $t_{s, \text{peak}}$, respectively. To quantify the peak position shift of $t_{s, \text{peak}}$ with respect to t_{peak} , we only need to compare their difference. In the following analysis, we define the difference as $\delta = t_{\text{peak}} - t_{s, \text{peak}}$.

Because the derivatives of $f(t_m)$ and $f_s(t_m)$ with respect to t_m are both equal to zero at the peak positions. Namely, we have equations

$$\left. \frac{df(t_m)}{dt_m} \right|_{t_m=t_{\text{peak}}} = 0, \quad (\text{B1})$$

$$\left. \frac{df_s(t_m)}{dt_m} \right|_{t_m=t_{s, \text{peak}}} = 0. \quad (\text{B2})$$

We first discuss the case as shown in Fig. 1. The true light curve profile $f(t_m)$ around the peak t_{peak} is concave, and the absolute value of the derivative on the left of the peak is larger than that on the right, namely,

$$\left. \frac{df(t_m)}{dt_m} \right|_{t_m < t_{\text{peak}}} > - \left. \frac{df(t_m)}{dt_m} \right|_{t_m > t_{\text{peak}}}. \quad (\text{B3})$$

If ε is a positive value, then the above inequality yields

$$f(t_{\text{peak}} - \varepsilon) < f(t_{\text{peak}} + \varepsilon). \quad (\text{B4})$$

In addition, substituting equation (2) into equation (B2), we can derive

$$f(t_{s, \text{peak}} - \Delta t/2) = f(t_{s, \text{peak}} + \Delta t/2). \quad (\text{B5})$$

Obviously, the equation only holds in the case of $t_{s, \text{peak}} - \Delta t/2 < t_{\text{peak}}$ and $t_{s, \text{peak}} + \Delta t/2 > t_{\text{peak}}$. It means that δ should satisfy

$$-\Delta t/2 < \delta < \Delta t/2. \quad (\text{B6})$$

Combing the equations (B4) and (B5), we further have

$$f(t_{\text{peak}} - \delta + \Delta t/2) = f(t_{\text{peak}} - \delta - \Delta t/2) < f(t_{\text{peak}} + \delta + \Delta t/2)$$

Because both $t_{\text{peak}} - \delta + \Delta t/2$ and $t_{\text{peak}} + \delta + \Delta t/2$ are larger than t_{peak} , immediately we get $t_{\text{peak}} - \delta + \Delta t/2 > t_{\text{peak}} + \delta + \Delta t/2$, i.e. $\delta < 0$. In summary, we have demonstrated that δ satisfies

$$-\Delta t/2 < \delta < 0. \quad (\text{B7})$$

The above inequality indicates that the peak position of $f_s(t_m)$ shifts rightwards with respect to the true peak position. And the offset is smaller than half of the exposure time.

Similarly, if the true light curve profile $f(t_m)$ around the peak t_{peak} is axisymmetric, e.g., the sine function, it is easy to prove that $\delta = t_{\text{peak}} - t_{s, \text{peak}} = 0$. If the rise phase before the peak is relatively flatter than the decay phase as opposed to the light curve shown in Fig. 1, the absolute value of the derivative on the left of the peak is expected to be smaller than that on the right. Following the same procedure, we can prove that $0 < \delta < \Delta t/2$. It means that the peak position of $f_s(t_m)$ shifts leftwards with respect to the true peak position. And the offset is also smaller than half of the exposure time.

APPENDIX C: TOTAL FLUX ESTIMATION OF STELLAR FLARE

Theoretically, the total integrated flux of a stellar flare is calculated through

$$f_{\text{tot}} = \int_{t_0}^{t_e} f(t) dt, \quad (\text{C1})$$

where t_0 and t_e denote the eruption start time and end time, respectively. Observationally, we can approximate f_{tot} by equation (8) where the time-averaged flux at $t_{m, i}$ is

$$f_s(t_{m, i}) = \frac{1}{\Delta t} \int_{t_{m, i} - \Delta t/2}^{t_{m, i} + \Delta t/2} f(t) dt. \quad (\text{C2})$$

Table D1. Best-fit parameters of the simulated stellar flare light curves.

Δt (s)	method	t_{peak} (minutes)	FWHM (minutes)	A
–	fiducial model	0.000	6.540	9.469
120	direct fit	0.144	6.992	8.942
	Δt involved	0.074	6.551	9.343
300	direct fit	0.025	8.746	7.624
	Δt involved	-0.057	6.770	9.249
600	direct fit	-1.947	7.037	12.044
	Δt involved	-0.171	6.773	9.432

To quantify the difference between f_{tot} and $f_{s,\text{tot}}$, we can expand equation (8) as

$$\begin{aligned}
 f_{s,\text{tot}} &= \sum_{i=1}^{n-1} \frac{f_s(t_{m,i}) + f_s(t_{m,i+1})}{2} \Delta t \\
 &= \Delta t \left[\frac{1}{2} f_s(t_{m,1}) + f_s(t_{m,2}) + \dots + f_s(t_{m,n-1}) + \frac{1}{2} f_s(t_{m,n}) \right] \\
 &= \Delta t \sum_{i=1}^n f_s(t_{m,i}) - \frac{1}{2} [f_s(t_{m,1}) + f_s(t_{m,n})] \Delta t. \quad (\text{C3})
 \end{aligned}$$

Under the assumption that there are no overheads or other gaps between two sequential exposures, we have $t_{m,i} + \Delta t/2 = t_{m,i+1} - \Delta t/2$. Therefore, combining the above three equations we can yield

$$f_{s,\text{tot}} = f_{\text{tot}} - \frac{1}{2} [f_s(t_{m,1}) + f_s(t_{m,n})] \Delta t. \quad (\text{C4})$$

As we have defined, the first exposure interval is $[t_{m,1} - \Delta t/2, t_{m,1} + \Delta t/2]$ and the relative offset between t_0 and $t_{m,1}$ is $\delta t_0 = t_{m,1} - t_0$. We expect that only a flare between t_0 and $t_{m,1} + \Delta t/2$ accounts for the flux budget of the first exposure. Likewise, for the last exposure, only flare between $t_{m,n} - \Delta t/2$ and t_e matters. Therefore, we finally have

$$f_{s,\text{tot}} = f_{\text{tot}} - \frac{1}{2} \left[\int_{t_{m,1} - \delta t_0}^{t_{m,1} + \Delta t/2} f(t) dt + \int_{t_{m,n} - \Delta t/2}^{t_{m,n} - \delta t_e} f(t) dt \right]. \quad (\text{C5})$$

The equation indicates that the presence of the relative offsets between t_0 and $t_{m,1}$ and between t_e and $t_{m,n}$ can cause potential underestimation of the total flux. Only under the extreme case that $t_0 = t_{m,1} + \Delta t/2$ and $t_e = t_{m,n} - \Delta t/2$, we have $f_{s,\text{tot}} = f_{\text{tot}}$.

APPENDIX D: STELLAR FLARE FITTING RESULTS

The best-fit parameters of the simulated stellar light curves are shown in Table D1.

This paper has been typeset from a $\text{\TeX}/\text{\LaTeX}$ file prepared by the author.